

From Magnets to Metals: The Response of Tetragonal Bisdiselenazolyl Radicals to Pressure

Alicea A. Leitch,[†] Kristina Lekin,[†] Stephen M. Winter,[†] Laura E. Downie,[‡] Hideki Tsuruda,[§] John S. Tse,^{||} Masaki Mito,[§] Serge Desgreniers,[‡] Paul A. Dube,[†] Sijia Zhang,[¶] Qingqing Liu,[¶] Changqing Jin,[¶] Yasuo Ohishi,[▽] and Richard T. Oakley*,[†]

[†]Department of Chemistry, University of Waterloo, Waterloo, Ontario N2L 3G1, Canada

[‡]Department of Physics, University of Ottawa, Ottawa, Ontario K1N 6N5, Canada

[§]Faculty of Engineering, Kyushu Institute of Technology, Kitakyushu 804-8550 Japan

^{||}Department of Physics and Engineering Physics, University of Saskatchewan, Saskatoon, Saskatchewan S7N 5E2, Canada

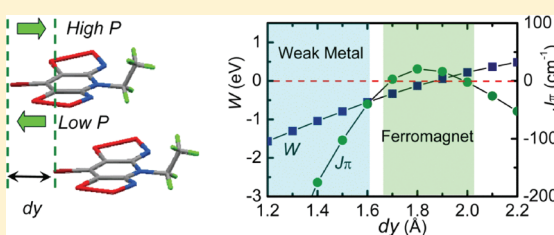
[†]Brockhouse Institute for Materials Research, McMaster University, Hamilton, Ontario L8S 4M1, Canada

[¶]Institute of Physics, Chinese Academy of Sciences, Beijing, 100080, China

[▽]Materials Science Division, Japan Synchrotron Radiation Research Institute (JASRI), SPring-8, Sayo, Hyogo 679-5198, Japan

Supporting Information

ABSTRACT: The bromo-substituted bisdiselenazolyl radical **4b** ($R_1 = Et$, $R_2 = Br$) is isostructural with the corresponding chloro-derivative **4a** ($R_1 = Et$, $R_2 = Cl$), both belonging to the tetragonal space group $P\bar{4}2_1m$ and consisting of slipped π -stack arrays of undimerized radicals. Variable temperature, ambient pressure conductivity measurements indicate a similar room temperature conductivity near $10^{-4} S \text{ cm}^{-1}$ for the two compounds, but **4b** displays a slightly higher thermal activation energy E_{act} (0.23 eV) than **4a** (0.19 eV). Like **4a**, radical **4b** behaves as a bulk ferromagnet with an ordering temperature of $T_C = 17.5$ K. The coercive field H_c (at 2 K) of 1600 Oe for **4b** is, however, significantly greater than that observed for **4a** (1370 Oe). High pressure (0–15 GPa) structural studies on both compounds have shown that compression reduces the degree of slippage of the π -stacks, which gives rise to changes in the magnetic and conductive properties of the radicals. Relatively mild loadings (<2 GPa) cause an increase in T_C for both compounds, that of **4b** reaching a maximum value of 24 K; further compression to 5 GPa leads to a decrease in T_C and loss of magnetization. Variable temperature and pressure conductivity measurements indicate a decrease in E_{act} with increasing pressure, with eventual conversion of both compounds from a Mott insulating state to one displaying weakly metallic behavior in the region of 7 GPa (for **4a**) and 9 GPa (for **4b**).



INTRODUCTION

Interest is growing in the development of organic radicals as building blocks for functional molecular materials,¹ that is, systems in which the unpaired electron associated with the radical serves as a carrier of charge and/or a magnetic coupler. From a synthetic perspective, the challenge is to design radicals with sufficient thermal stability to allow for detailed physical property measurements, while from a materials viewpoint attention focuses on the need to understand and hence modify their electronic and magnetic structures. If, for example, the unpaired electron is strongly localized, as in light heteroatom radicals such as nitroxyls, verdazyls, and thiazyls, conductivity is low. Moreover, through-space intermolecular magnetic exchange interactions are generally weak, and magnetic ordering is rare. A number of canted antiferromagnets have been generated,² but bulk ferromagnets have been more elusive,³ and for none of these has the coercive field amounted to more than a few Oersted.⁴ Nonmetal based radical ion salts displaying higher ferromagnetic ordering temperatures (T_C) have also been reported,⁵ with

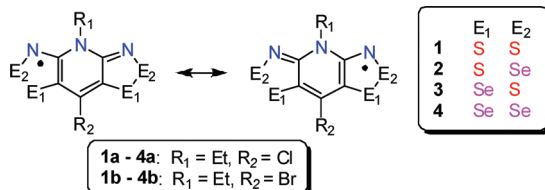
that of the TDAE·C₆₀ complex ($T_C = 16$ K) being the highest,⁶ but in these systems also the coercive field is very small.

If the extent of charge correlation can be diminished, charge transport along an array of weakly interacting radicals becomes possible.⁷ The solid state electronic structure of such systems is best described in terms of the half-filled band ($f = 1/2$) Mott–Hubbard model,^{8,9} with one electron associated with each radical site. Within this context, high conductivity requires that intermolecular interactions, expressed in terms of the nearest neighbor resonance integral β , be maximized, and that the barrier to charge transport, the Mott–Hubbard onsite Coulomb potential U , be minimized. In principle, a metallic state should prevail when the electronic bandwidth W ($= 4\beta$) is sufficient to offset the Coulomb potential, that is, when $W > U$.¹⁰ In addition to the charge correlation issue, all radicals suffer from a tendency to

Received: January 26, 2011

Published: March 28, 2011

Chart 1

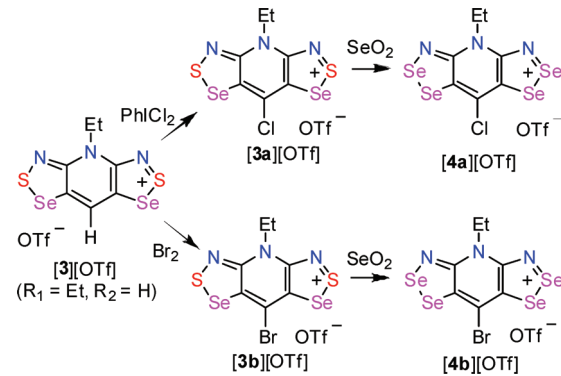


dimerize in the solid state, either through localized σ -bonds or multicenter $\pi-\pi$ interactions.¹¹ Association has the effect of quenching magnetic properties, and can lead to a loss in conductivity which, in π -stacked structures, may be rationalized in terms of a charge-density-wave or Peierls distortion.¹² In light of these issues, synthetic efforts aimed at producing conductive radical-based materials have focused on (i) the use of highly delocalized organic systems, notably phenalenyls and spirophenalenyls,^{13,14} which enjoy a low value of U , and (ii) the incorporation of heavy (soft) heteroatoms,¹⁵ which can lead to an enhanced bandwidth W . While progress has been made in suppressing dimerization, the correlation problem remains unresolved; the isolation of a neutral radical conductor, indeed any organic $f = 1/2$ conductor, displaying a metallic ground state has yet to be achieved.

In recent years, our work on functional radicals has involved resonance stabilized heterocycles of the type **1–4** (Chart 1). These highly delocalized spin systems, which display low gas phase disproportionation energies ΔH_{disp} and electrochemical cell potentials E_{cell}^{10} indicative of a low onsite Coulomb potential U , were designed to allow for alteration in both intermolecular magnetic and electronic interactions either through variations in the exocyclic substituents R_1 and R_2 ,¹⁷ or through replacement of sulfur by its heavier (and softer) congener selenium.¹⁸ The ability to incorporate selenium proved to be doubly effective, leading not only to significant enhancements in conductivity, by virtue of the greater spatial extension of 4p-orbitals on selenium relative to 3p-orbitals on sulfur, but also to some remarkable magnetic effects. Compounds **3** and **4** ($R_1 = \text{Et}$, $R_2 = \text{H}$), for example, were found to order as spin-canted antiferromagnets with T_N values of 18 and 27 K, respectively,¹⁹ while **2** and **4** ($R_1 = \text{Et}$, $R_2 = \text{Cl}$) were observed to order as bulk ferromagnets with T_C values of 12.8 and 17 K.²⁰ In addition to their high ordering temperatures, the latter two materials were found to display coercive fields H_c (at 2 K) of 250 and 1370 Oe.

While the observation of a single component molecular material displaying ferromagnetic ordering along with conductivity represents a significant advance in the pursuit of molecular spintronics,²¹ improvements in conductivity, ordering temperature, and coercivity require a better understanding of the relationship between crystal structure, electronic structure, and bulk property.²² With this in mind, we explored the effect of variations in the molecular packing found for **2a**, using minor modifications of the R_1/R_2 groups such that the tetragonal space group ($P\bar{4}2_1m$) of **2a** was preserved. Four isostructural variants, differing only in the degree of slippage of the radicals along the π -stacking direction, were examined. While two of the modifications (**2**: $R_1 = \text{Et}$; $R_2 = \text{Me}, \text{Br}$) ordered as ferromagnets, with T_C and H_c values close to those of **2a**, the other two (**2**: $R_1 = \text{CH}_2\text{CF}_3, \text{Pr}$; $R_2 = \text{Cl}$) showed no indication of ordering above 2 K.²³ This study illustrated the use of *chemical pressure*, that is, the introduction of a small perturbation by synthetic means, to modify structure and hence property. An alternative

Scheme 1



strategy is to invoke *physical pressure*,²⁴ and in this regard we recently showed that both the crystal structure and ordering temperature of **4a** could be modified by the application of relatively mild pressures.²⁵ However, the slight increase in T_C provided by pressures <1 GPa was followed by a decrease in T_C at more elevated pressures. These changes were correlated with a decrease in slippage of the π -stacks, a process which produced an initial increase and then a subsequent decrease in the (calculated) pairwise intermolecular magnetic exchange interaction along the π -stacks.

One of the implications of this result is that with continued slippage and compression of the π -stacks of **4a**, there should be a marked increase in intermolecular overlap and hence electronic bandwidth. We have therefore examined the effect of increased pressure (beyond 5 GPa) on the crystal structure and charge transport properties of **4a**. For purposes of comparison, we have prepared and characterized the isostructural bromo-substituted bisdiselenazolyl **4b** ($R_1 = \text{Et}$, $R_2 = \text{Br}$). It too is a bulk ferromagnet, with T_C near 17 K, and with relatively mild compression (<5 GPa) it undergoes similar structural and magnetic changes to those observed for **4a**, but the maximum T_C (24 K at 2 GPa) is higher. In addition, variable temperature conductivity and structural measurements on both compounds reveal that compression beyond the region where magnetic ordering is quenched, that is near 7 GPa for **4a** and 9 GPa for **4b**, is sufficient to induce weakly metallic behavior. This latter finding represents, to our knowledge, the first observation of pressure-induced metallization of a neutral radical conductor.

RESULTS

Synthesis. The synthesis of **4b** is based on the procedure previously developed for the preparation of **4a**.²⁰ The starting material for both compounds is the triflate (OTf^-) salt of the bis-1,2,3-selenathiazolyl cation $[3]^+$ ($R_1 = \text{Et}$, $R_2 = \text{H}$). Oxidation of this material with iodobenzene dichloride (Scheme 1) affords the triflate salt of the chloro-substituted cation $[3a]^+$, while the use of bromine or *N*-bromosuccinimide yields the corresponding bromo-derivative $[3b][\text{OTf}]$. Subsequent treatment of these two salts with selenium dioxide in boiling acetic acid leads to sulfur/selenium exchange and the formation of the respective all-selenium salts $[4a, b][\text{OTf}]$. Bulk reduction of these compounds, to produce the respective radicals **4a,b** in microcrystalline form suitable for ambient and high pressure transport property measurements can be conveniently effected with *N,N,N',N'*-tetramethyl-p-phenylenediamine or octamethylferrocene. Single crystals of the radicals suitable for X-ray diffraction are best grown by electrocrystallization methods.

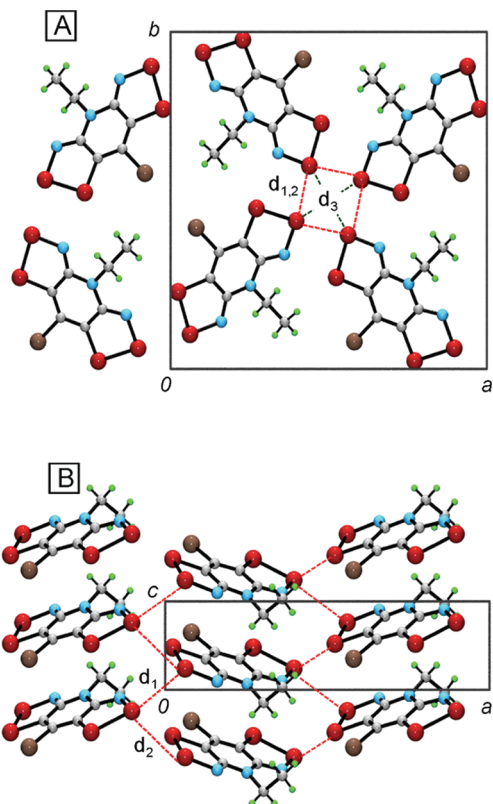


Figure 1. Crystal packing of **4b**, viewed parallel to the *c*-axis (A) and *b*-axis (B). Intermolecular contacts $\text{Se} \cdots \text{Se}'$ contacts d_1 , d_2 , and d_3 are shown with dashed lines.

Table 1. Crystal Data and Metrics for 4a,b

	4a ^a	4b
formula	$\text{C}_7\text{H}_5\text{ClN}_3\text{Se}_4$	$\text{C}_7\text{H}_5\text{BrN}_3\text{Se}_4$
<i>M</i>	482.43	526.89
<i>a</i> (\AA)	16.2708(5)	16.3109(14)
<i>c</i> (\AA)	4.1720(3)	4.1753(7)
<i>V</i> (\AA^3)	1104.49(9)	1110.8(2)
ρ_{calcd} (g cm^{-3})	2.901	3.151
space group	$P\bar{4}2_1m$	$P\bar{4}2_1m$
<i>Z</i>	4	4
temp (K)	296(2)	296(2)
μ (mm^{-1})	13.494	16.774
λ (\AA)	0.71073	0.71073
data/restr./parameters	1209/0/76	1211/0/76
solution method	direct methods	direct methods
R, R_w (on F^2)	0.0374, 0.0635	0.0307, 0.0504
Se_1-Se_2 (\AA)	2.3614(10)	2.3604(9)
Se_2-N (\AA)	1.829(5)	1.827(5)
Se_1-C (\AA)	1.868(6)	1.875(6)
d_1 (\AA)	3.404(1)	3.411(1)
d_2 (\AA)	3.502(1)	3.519(1)
d_3 (\AA)	3.891(1)	3.910(1)
δ (\AA)	3.567	3.563
dy (\AA)	2.164	2.178
deviation from plane (\AA) ^b	0.0843	0.0287

^a Data from reference 20b. ^b Mean value of deviations of all atoms from plane of heterocyclic framework.

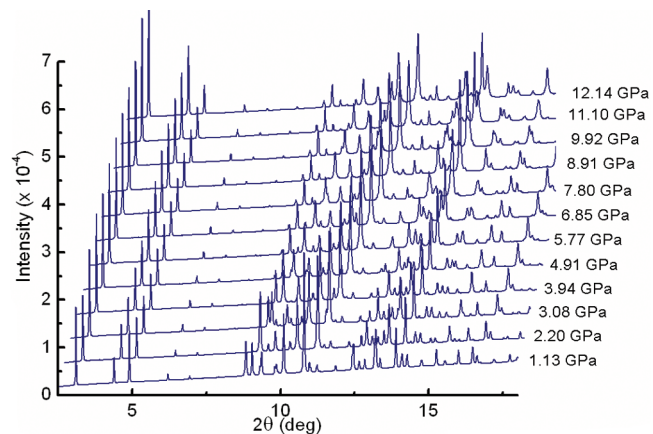


Figure 2. Powder diffraction data ($\lambda = 0.61795 \text{ \AA}$) for **4b** as a function of applied pressure.

Crystallography. Single crystal X-ray diffraction has established that **4b** is isomorphous with **4a**,²⁰ both compounds belonging to the tetragonal space group $P\bar{4}2_1m$. The two crystal structures consist of radicals bisected by (110) mirror planes and arranged in pinwheel-like clusters about the $\bar{4}$ centers of the unit cell. The radicals pack into slipped π -stack arrays running parallel to the *c*-axis, as may be seen in Figure 1, which illustrates the unit cell of **4b** viewed parallel and perpendicular to the stacking direction. Crystal metrics for the two compounds at ambient pressure are provided in Table 1. There are numerous intermolecular $\text{Se} \cdots \text{Se}'$ contacts, notably d_1 , d_2 , and d_3 , that are close to or within the nominal van der Waals separation for selenium.²⁶

Having established the crystal structures of both **4a** and **4b** at ambient pressure, we wished to explore the effect of physical pressure on the molecular packing, so as to be able to rationalize any changes in transport properties with pressure. To this end high pressure powder diffraction data on both compounds were collected at room temperature as a function of increasing pressure using synchrotron radiation and a diamond anvil cell, with helium as the pressure transmitting medium. Sets of diffraction data up to 15 GPa on each compound were indexed and the structures solved in DASH using molecular models derived from the ambient pressure single crystal solutions. As may be seen in Figure 2, which shows the data sets collected on **4b** over the pressure range 1–12 GPa, the retention of resolution and the smooth and steady evolution of the positions of the diffraction peaks with increasing pressure indicates that no phase change has occurred as a result of compression, and that there has been no degradation of the sample. During the initial Rietveld refinement, performed using DASH, a rigid-body constraint was maintained. The final Rietveld refinement of the unit cell, with fixed atomic positions and isotropic thermal parameters, was carried out using GSAS. Changes in the unit cell parameters as a function of pressure for **4a,b** are illustrated in Figure 3.

While compression of the unit cells of **4a** and **4b** does not alter the space group or the packing of the radical π -stacks about the $\bar{4}$ points along the *c*-direction, it does alter the canting of the π -stacks. The extent of these changes may be conveniently defined (Figure 4 and Table 1) in terms of the degree of slippage (dy) of neighboring radicals. As shown in Figure 5, the value of dy decreases with increasing pressure; in essence the radical π -stacks become more nearly superimposed. At the same time the interplanar separation (δ) between adjacent radicals is also reduced. If there

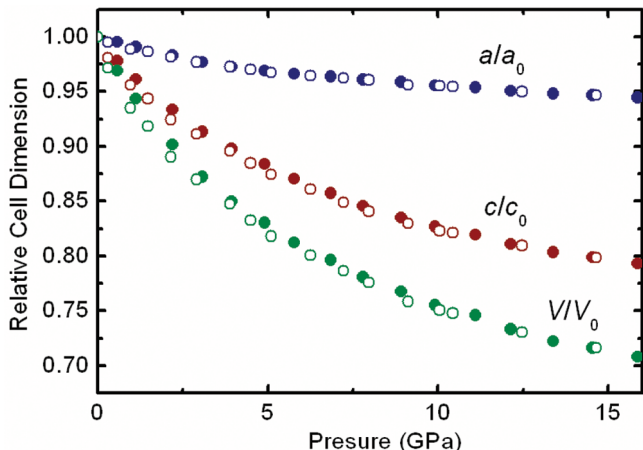


Figure 3. Cell dimensions (relative to values at 0 GPa) of the unit cell parameters of **4a** (open circles) and **4b** (closed circles) as a function of pressure.

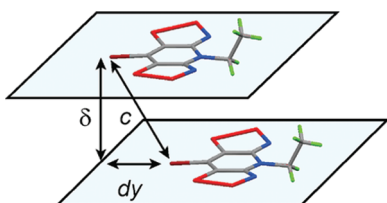


Figure 4. Slippage (dy) and interplanar separation (δ) of adjacent radicals along the π -stacks of **4a,b**.

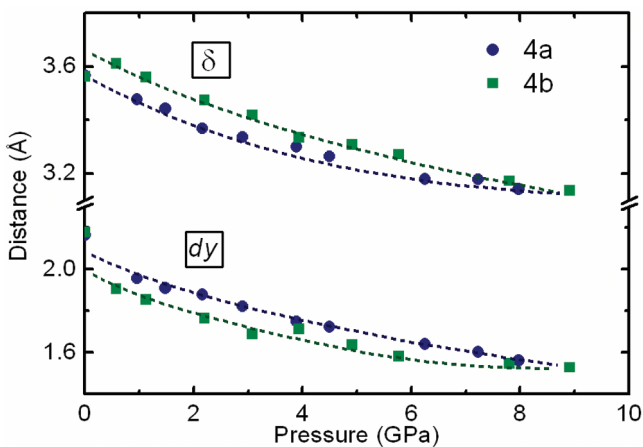


Figure 5. Variations in the intermolecular metrics δ and dy in **4a** and **4b** with pressure.

is any difference in the response of the two structures, stack spacing δ is, at low pressures, slightly larger for **4b** than for **4a**, while the slippage parameter dy is smaller (the stacks are more nearly superimposed). By 10 GPa, however, the values of both δ and dy for the two compounds have essentially coalesced, as expected. Lateral compression along the a and b directions causes a shortening of the intermolecular contacts d_1 , d_2 , and d_3 ; the resulting trends are illustrated in the Supporting Information. The collective effects of all these structural changes on the magnetic and conductive properties of the two compounds are described below.

Magnetic Measurements. Ambient pressure magnetic susceptibility χ measurements on **4b** reveal similar results to those

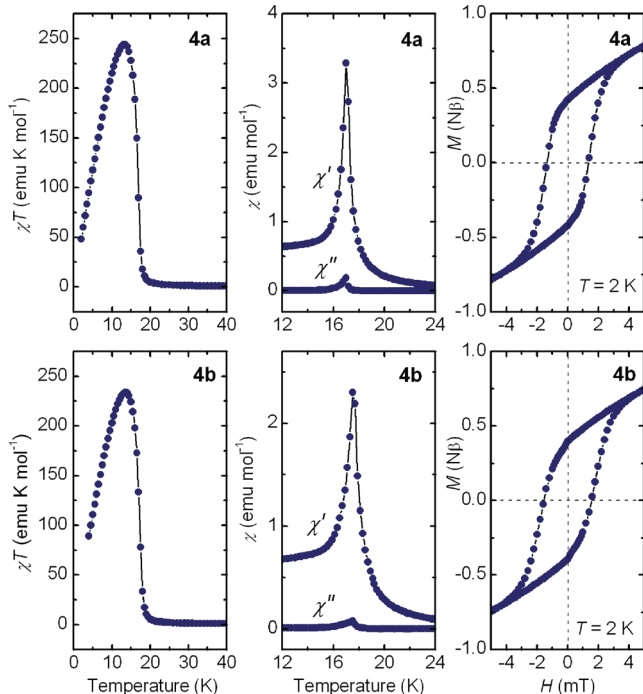


Figure 6. Plots of χT (field-cooled) versus temperature at 100 Oe (left) for **4a** and **4b** at ambient pressure, along with plots of the AC susceptibility χ' and χ'' versus temperature at 1 kHz (center) and magnetization M versus field at $T = 2$ K (right).

Table 2. Ambient Pressure Magnetic and Conductivity Data

	4a ^a	4b
C (emu K mol ⁻¹)	0.392	0.387
θ (K)	22.9	23.2
T_C (K)	17.0	17.5
M_{sat} (N β) at 2 K	1.03	1.02
M_{rem} (N β) at 2 K	0.41	0.40
H_c (Oe) at 2 K	1370	1600
σ (300 K) (S cm ⁻¹)	3.0×10^{-4}	6.0×10^{-4}
E_{act} (eV)	0.19	0.23

^a Data from reference 20b.

previously reported for **4a**.²⁰ Plots of χT (field cooled) versus temperature at a field of $H = 100$ Oe (Figure 6, left) confirm that both compounds behave as paramagnets between 50 and 300 K, with χT (300 K) values of 0.432 (**4a**) and 0.420 emu K mol⁻¹ (**4b**). Curie–Weiss fits to the data (corrected for diamagnetic contributions)²⁷ afford Curie constants C of 0.369 and 0.387 emu K mol⁻¹, respectively (Table 2), that is, near the value expected (0.375 emu K mol⁻¹) for an $S = 1/2$ system with g nominally equal to 2. The large positive Weiss constants θ of 22.9 (**4a**) and 23.2 K (**4b**) indicate the presence of strong local ferromagnetic exchange interactions. Upon cooling both compounds there is a slow rise in χT , in keeping with the positive θ -values, followed by a dramatic surge just below 20 K, with χT reaching a maximum of 244 emu K mol⁻¹ near 14 K for **4a** and 232 emu K mol⁻¹ for **4b**.²⁸ This response is consistent with a phase transition to a ferromagnetically ordered state. At temperatures below these maxima, there is a steady drop-off in χT for both compounds, as would be expected from low temperature

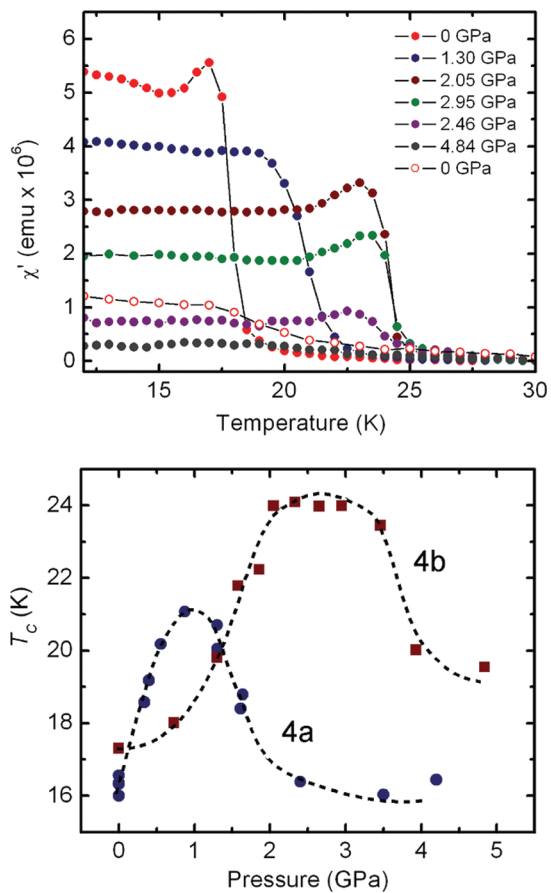


Figure 7. Plots of χ' , the in-phase component of the AC susceptibility (at 10 Hz), versus temperature for **4b** at different pressures (above) and of T_C versus pressure for both **4a** and **4b** (below). The lower trace at 0 GPa in the χ' versus T plots is from a postpressurization measurement.

magnetization saturation. Variable temperature AC susceptibility measurements at different frequencies allow us to pinpoint and compare the ordering temperatures T_C of the two compounds. As shown in Figure 6 (center), both radicals show sharp, well-defined maxima in the real (in-phase) χ' and imaginary (out-of-phase) χ'' components at 17.0 K (**4a**) and 17.5 K (**4b**). The invariance of T_C with changes in the cycling frequency (from 100 Hz to 5 kHz) establishes that these materials are not spin glasses.

Magnetization (M) measurements as a function of field show that for both compounds M rises sharply with H , reaching a maximum (at 2 K) at $H = 10$ kOe, after which there is no further change up to $H = 55$ kOe; the saturation magnetization values M_{sat} of 1.03 (**4a**) and 1.02 N β (**4b**) are in accord with a $S = 1/2$ system with a nominal g value of 2.²⁹ Reversal and cycling of the field sweep leads to hysteresis. Plots of M versus H , from measurements at 2 K (Figure 6, right) show that while the remanent magnetization M_{rem} of the two compounds is virtually the same, the coercive field H_c of **4b** (1600 Oe) is noticeably greater than found for **4a** (1370 Oe), a difference which may be a result of increased magnetic anisotropy occasioned by a larger spin–orbit coupling contribution from bromine.

In our initial communication, we explored the effect of physical pressure on the magnetic properties of **4a** by means of DC and AC magnetic susceptibility measurements performed over the pressure range 0–1.6 GPa under hydrostatic conditions using a piston cylinder cell (PCC) in a SQUID magnetometer.²⁵ The results

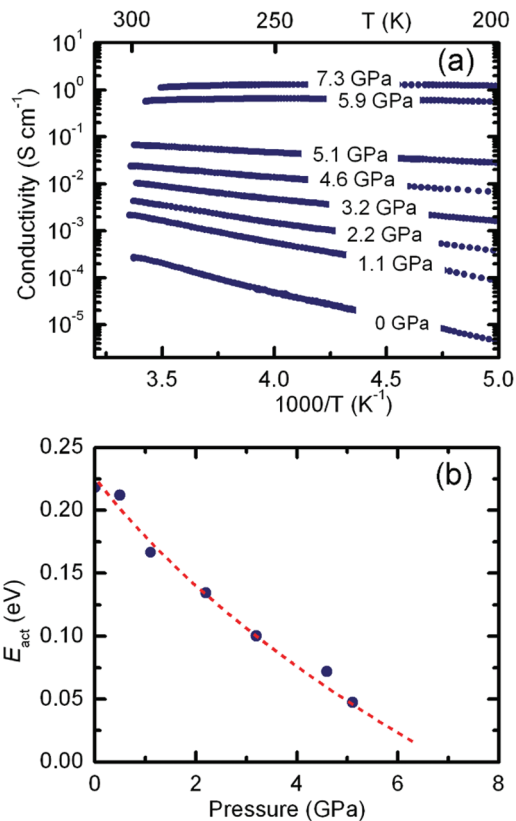


Figure 8. (a) Log plot of σ versus $1/T$ for **4a** at different pressures, for $T = 200$ –300 K. (b) Thermal activation energy E_{act} for **4a** as a function of pressure over the range $T = 200$ –300 K (below).

indicated an initial increase in the ferromagnetic ordering temperature T_C to a maximum value of 21 K near 0.9 GPa. Beyond this pressure, T_C retreated, so that by 1.6 GPa its value was near 18 K. Similar results were obtained using the quasi-hydrostatic compression afforded by a diamond anvil cell (DAC). The latter technique also allowed access to pressures above 1.6 GPa and revealed a continued decrease in T_C to 16 K at 2 GPa, with little change thereafter to the limit of the experiment (4 GPa). The magnetic response was also significantly reduced at higher pressures, suggesting at least a partial collapse of the ferromagnetic network^{24,30} and/or the possibility of the formation of an antiferromagnetically (AFM) ordered state (vide infra). We have now examined the change in the value of T_C of **4b** over the pressure range 0–5 GPa, by means of AC susceptibility measurements recorded using a DAC. As illustrated in Figure 7, the dependency of T_C on pressure follows a similar profile to that found for **4a**, although the increase in T_C is more gradual and the maximum value is near 24 K, which is substantially larger than that found for **4a**. Moreover, this maximum is preserved over the pressure range 2–4 GPa. As observed for **4a**, the magnitude of χ' drops sharply beyond the plateau region, suggesting a breakdown of the long-range ferromagnetic (FM) network or a reversal of the ordering from FM to AFM. There is, however, a partial recovery in the moment (and T_C) when the pressure is released, suggesting the re-establishment of the FM ordered state.

Conductivity Measurements. As in our previous work on **4a**, we have measured the ambient pressure conductivity σ of **4b** over the temperature range 200–300 K, using the 4-probe method on a pressed pellet sample; values of $\sigma(300 \text{ K})$ and the thermal activation energy E_{act} for both compounds derived from

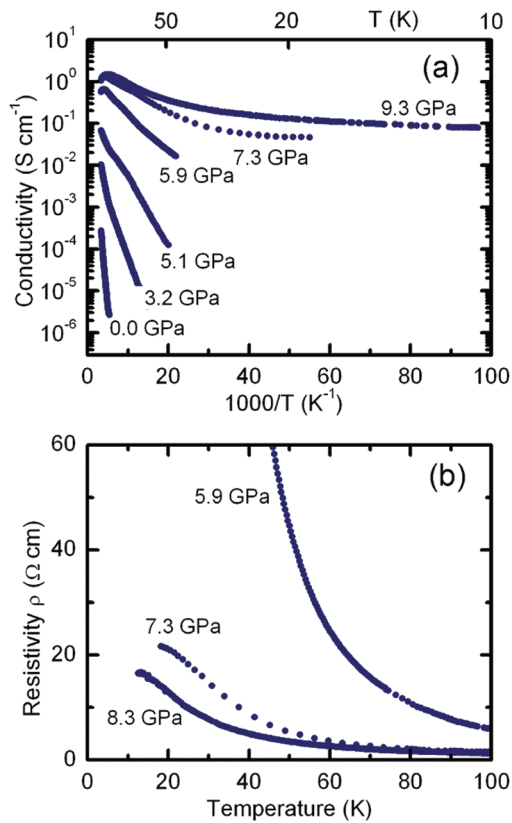


Figure 9. (a) Log plots of σ versus $1/T$ for **4a** at different pressures, for $T = 10\text{--}300\text{ K}$. (b) Plots of resistivity ρ versus T for **4a** at different pressures (below).

Arrhenius fits are listed in Table 2. In order to explore the changes in both conductivity and activation energy with pressure, we turned to the use of diamond anvil cell techniques. These measurements did not afford conductivity values directly, as it was not possible to obtain accurate measurements of sample dimensions, but we were nonetheless able to effect the conversion by calibrating the DAC resistance data with the conductivity values taken from the ambient pressure measurements. As may be seen in Figure 8, the decrease in $\log \sigma$ with $1/T$ for **4a** is approximately linear from 200 to 300 K over the pressure range 0–5 GPa; for **4b**, this pseudolinear range extends out to about 8 GPa (plots of conductivity data for **4b** are provided in the electronic Supporting Information). Arrhenius fits to the data within these confines affords thermal activation energies E_{act} which decrease steadily with pressure, and extrapolation suggests that its value would reach 0 eV near 7 GPa for **4a** (near 9 GPa for **4b**). The theoretical and experimental challenge then becomes one of establishing whether the apparent elimination of a thermal barrier to activation heralds the onset of a metallic state.

To explore this issue, we examined the conductivity of both compounds in the low temperature region. As may be seen in Figure 9a, which expands the $\log \sigma$ versus $1/T$ plots for **4a** over the temperature range 10–300 K, the conductivity drops rapidly with decreasing temperature for pressures ≤ 5.9 GPa, as would be expected for activated (nonmetallic) conductivity; for **4b** this range extends out to 7.7 GPa. By contrast, at more elevated pressures, that is ≥ 7.3 GPa for **4a** (and ≥ 9.4 GPa for **4b**), $\log \sigma$ does not tend to zero, but instead settles to a plateau value in the low temperature limit. This phenomenon, the apparent loss of

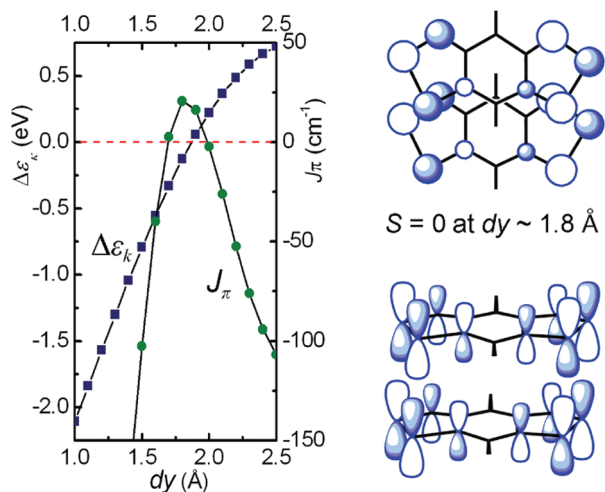


Figure 10. DFT estimated J_π values and EHT band dispersion energy $\Delta\epsilon_k$ (where $|\Delta\epsilon_k| = W$) for a 1D π -stack of a model **4** ($R_1 = R_2 = H$) as a function of dy with $\delta = 3.5\text{ \AA}$ (left). For full details of these calculations, see refs 22 and 23. Also shown is the SOMO–SOMO overlap S at $dy \sim 1.8\text{ \AA}$ viewed from above and side.

thermal activation, can also be illustrated by means of a plot of the resistivity ρ against temperature in the critical pressure region where E_{act} approaches zero. As is apparent in Figure 9b, the resistivity rises asymptotically with decreasing temperature for all pressures ≤ 5.9 GPa for **4a**, as would be expected for a nonmetallic material in which all charge carriers are lost at 0 K. However, at pressures near and above 7.3 GPa, ρ appears to saturate as the temperature is decreased. In fact, below 25 K the rate of increase in ρ diminishes and extrapolation of the data indicates convergence to a finite value of ρ at $T = 0\text{ K}$, an observation consistent with the onset of a weakly metallic state, that is, one in which charge carriers are present at 0 K. A similar situation is found for **4b**, only the crossover from a formally nonmetallic to weakly metallic state occurs somewhere between 7.7 and 9.4 GPa (see electronic Supporting Information).

DISCUSSION

Physical pressure has been widely used to explore the metal to Mott insulator (MI) transition in metal oxides and chalcogenides³¹ and also in organic charge transfer compounds such as the κ -phase salts of BEDT-TTF and Beechgard salts [$\text{TMTSF}]_2[\text{X}]$.³² In the latter systems, where the MI energy gap can be quite small, a rich array of phases, ranging from paramagnetic insulating to antiferromagnetic insulating, metallic, and even superconducting can be accessed. Moreover, as a result of the higher compressibilities of organic charge transfer salts relative to inorganic materials, the interconversion of these states often occurs with relatively mild (<1 GPa) compression. By contrast, metallization of **4a** and **4b** require somewhat greater pressures, in the region of 7–9 GPa, despite their displaying small activation energies. This may reflect the fact the radicals are more tightly packed single component materials, but also may be attributed to increased correlation arising from their $f = 1/2$ structure. En route to the MI transition, the magnetic properties of the two radicals undergo a series of changes. For both compounds, the initial pressure-induced decrease in the slippage of the π -stacks leads to an increase in the ferromagnetic ordering temperature T_C , one more pronounced for **4b**, which displays a maximum and, to our knowledge, record value of $T_C = 24\text{ K}$ at

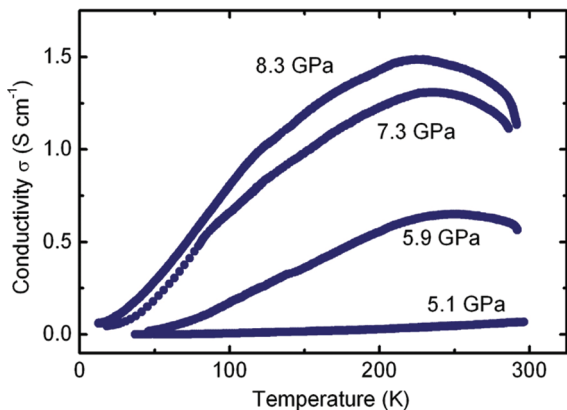


Figure 11. Conductivity of **4a** as a function of temperature in the region of the pressure induced MI phase transition, showing the progression from bad metal ($T \sim 20$ K) to Mott insulator ($T = 20\text{--}200$ K) to pseudometallic transport ($T > 200$ K).

2 GPa. With further compression, however, T_C retreats, and the magnetization weakens, so that by 5 GPa the ferromagnetic response of both materials appears to be completely quenched.

A qualitative explanation for both the initial increase and subsequent decrease in T_C can be conveniently developed using the orbital overlap arguments prescribed by Kahn, which emphasize the importance of an orthogonal overlap condition for ferromagnetic coupling.³³ Within this context, we demonstrated in earlier computational analyses^{22,23} that the most structurally sensitive intermolecular magnetic exchange interaction in these materials is the intrastack term J_π , the value of which rises and falls as the SOMO–SOMO interaction between adjacent radicals in the π -stack moves through a region of orthogonal overlap. The magnitude of these changes was estimated²³ using DFT-based methods³⁴ to calculate J_π for an idealized 1D array of bisdiselenazolyl radicals **4** ($R_1 = R_2 = H$) as a function of the pressure dependent π -stack slippage parameter dy .³⁵ The resulting variations in J_π for this model system, which are shown in Figure 10, reveal that both its sign and magnitude, and hence the conditions for FM versus AFM ordering, are critically dependent on the value of dy , and hence applied pressure. The computed value of J_π is, indeed, only ferromagnetic (positive) over a relatively small range (1.7–2.0 Å) of dy . Within this context it is notable that while compounds **2a,b** and **4a,b** order ferromagnetically, the related derivatives **3a,b** both order as spin-canted antiferromagnets.³⁶ The only difference between the three pairs is the value of J_π , which DFT calculations suggest is more negative (AFM) for **3a,b** than for either **2a,b** or **4a,b**. Thus, the marked decrease in magnetization of **4a,b** above 2 GPa may eventually lead to a turnover from FM to AFM ordering as dy decreases to values less than 1.7 Å. While further experiments and/or calculations are required to substantiate or refute this possibility, we note that pressure-induced reversals in ordering have been observed in nitroxyl radicals³⁰ and in the salts of thiazyl radical cations.³⁷

The orbital overlap-based arguments outlined above for correlating structure and magnetic property also afford a qualitative insight into the changes in conductivity that occur with continued compression. Thus, comparison (Figure 10) of the 1D-dispersion energy $\Delta\varepsilon_k$ (where $|\Delta\varepsilon_k| = W$)³⁸ for the same idealized array of **4** ($R_1 = R_2 = H$) suggests that pressures beyond 5 GPa, which induce decreases in π -stack slippage to values of $dy \sim 1.5$ Å, should induce a significant enhancement in W . Such an

increase, when coupled with the band broadening expected to arise from compression of the π -stacks, that is, a reduction in δ , also implies that the loss of ferromagnetic ordering, be it followed or not by the onset of AFM ordering, should eventually lead to metallization. Experimentally, this condition is found to occur near 7 GPa for **4a** and 9 GPa for **4b**.

Regarding the nature of the metallic state observed for **4a** and **4b**, we note that the low-pressure saturation values of the resistivity of both compounds are several orders of magnitude larger than the Mott–Ioffe–Regel limit,^{32d,39} $\rho = (\hbar/e^2)\delta \sim 10^{-4} \Omega \text{ cm}$, taking $\delta = 3.5$ Å. At this time, we therefore classify the low T (~ 20 K), high P state as an incoherent “bad metal” state, characterized typically by an anomalously high resistivity for a metallic conductor, but one that does not diverge as T approaches 0 K. Assuming that the material does exhibit a true Fermi liquid (normal metallic) ground state, this observation can be rationalized by application of Dynamical Mean Field Theory to the Hubbard model at half-filling.⁴⁰ In this approach, a Fermi liquid is expected to prevail at $T = 0$ K provided that $W > U$ but will give way to a bad metallic state as the temperature exceeds a coherence scale, analogous to what is observed in some Kondo lattice compounds.⁴¹ However, due to the lack of high pressure conductivity data below 10 K, we are reluctant at this time to refer to the $T = 0$ K state for **4a** and **4b** as a true Fermi liquid. That being said, the resistivity plateau and subsequent region of activated conductivity ($d\sigma/dT > 0$) for $T > 20$ K is broadly consistent with the theoretical predictions. As the temperature is further increased, a conductivity maximum is found, as T exceeds the energy scale for charge density fluctuations, that is, the Mott–Hubbard gap. Above this temperature of maximum conductivity ($T \sim 200$ K for both **4a** and **4b**; see Figure 11), phonon scattering should dominate such that $d\sigma/dT < 0$. Similar variations in transport properties have been observed in many other highly correlated metals, such as the high pressure phase of κ -(BEDT-TTF) salts,³² as well as Kondo lattice compounds such as CeAl₃ and CeCu₆.⁴¹

SUMMARY

The magnetic and charge transport properties of radicals **4a** and **4b** are unique. At ambient pressure both materials are bulk ferromagnets with the highest T_C values found outside of transition-metal based materials, display coercive fields that are several orders of magnitude greater than other radical ferromagnets, and also possess appreciable, albeit activated, conductivity. The high pressure structural measurements presented here provide a clear view of the response of the crystal structure of both materials to *physical pressure* and have allowed for the development of a qualitative understanding of the evolution of their solid state electronic and magnetic properties with compression. At ambient pressure, slippage of the radical π -stacks produces almost perfectly orthogonal overlap between adjacent SOMOs. The consequent FM exchange interactions along the π -stacks, when combined with FM exchange interactions lateral to the π -stacks, give rise to ferromagnetically ordered systems. Changes in slippage and plate-to-plate separation of the π -stacks occasioned by compression first enhance and then destroy the orthogonal overlap condition, so that exchange interactions along the π -stacks become strongly antiferromagnetic. As a result ferromagnetic ordering is lost, and possibly replaced by an AFM ordered state at intermediate pressures. Continued pressurization eventually generates sufficient bandwidth W to overcome the onsite Coulomb repulsion energy U . The onset of weakly

metallic behavior for **4a** and **4b** at pressures near 7 and 9 GPa, respectively, represent, to our knowledge, the first observation of a pressure-induced generation of such a state for a neutral radical ($f = 1/2$) material. It remains to be seen whether *chemical* modifications of these or related radicals will allow for the full metallization condition ($W > U$) to be met at lower pressures, or perhaps even under ambient conditions. The possibility that superconductivity may be found in these kinds of materials, with or without the need for applied pressure, provides an additional impetus for further exploration.

■ EXPERIMENTAL SECTION

General Procedures and Starting Materials. The reagents selenium dioxide, bromine, *N*-bromosuccinimide, silver trifluoromethanesulfonate (triflate, OTf⁻), and *N,N,N',N'*-tetramethyl-*p*-phenylenediamine (TMEDA) were obtained commercially. TMEDA was purified by sublimation in *vacuo*. Compound [3][OTf] (R₁ = Et, R₂ = H) and radical **4a** were prepared according to literature methods.²⁰ The solvents acetonitrile (MeCN), dichloroethane (DCE), acetic acid (HOAc), and dichloromethane (DCM) were of at least reagent grade. MeCN was dried by distillation from P₂O₅ and/or CaH₂, and both DCE and DCM by distillation from P₂O₅. All reactions were performed under an atmosphere of dry nitrogen. Infrared spectra (Nujol mulls, KBr optics) were recorded on a Nicolet Avatar FTIR spectrometer at 2 cm⁻¹ resolution. Low resolution Electro-Spray Ionization (ESI) mass spectra were run on a Micromass Q-TOF Ultima Global LC/MS/MS system. Elemental analyses were performed by MHW Laboratories, Phoenix, AZ 85018.

Preparation of 8-Bromo-4-ethyl-4H-bis[1,2,3]selenathiazolo[4,5-*b*:5',4'-*e*]pyridin-2-ium Triflate, [3b][OTf]. Method 1. Bromine (0.35 mL, 6.81 mmol) was added to a slurry of [3][OTf] (R₁ = Et, R₂ = H) (2.50 g, 4.97 mmol) in 250 mL MeCN and the reaction mixture was slowly heated to reflux. After 3 h the slurry was cooled slightly and the precipitate of [3b][Br] was filtered off in *vacuo* and washed 2 × 60 mL MeCN, yield 1.49 g (2.90 mmol, 58%). IR: 1490 (m), 1448 (s), 1423 (s), 1346 (s), 1184 (m), 1086 (w), 1069 (w), 987 (w), 871 (m), 830 (m), 797 (m), 786 (m), 700 (s), 647 (s), 578 (m), 531 (s), 499 (s) cm⁻¹. Silver triflate (0.82 g, 3.19 mmol) was added to a slurry of [3b][Br] (1.49 g, 2.90 mmol) in 200 mL MeCN to give a green slurry that was warmed at about 60 °C for 1 h. The reaction mixture was hot-filtered through paper to remove AgBr. The filtrate was concentrated to 100 mL and then cooled slowly to room temperature. The red solid of [3b][OTf] was filtered off and washed with 40 mL DCM, yield 1.32 g (2.26 mmol, 78%).

Method 2. A slurry of [3][OTf] (R₁ = Et, R₂ = H) (1.85 g, 3.67 mmol) and *N*-bromosuccinimide (0.850 g, 4.78 mmol) in 150 mL MeCN was heated slowly to reflux and after boiling for 90 min the resulting solution was filtered hot through a fine (E porosity) frit. The filtrate was cooled slowly to room temperature and then at -20 °C for 16 h. The red solid of [3b][OTf] was filtered off and washed with 30 mL DCM, yield 1.00 g (1.72 mmol, 47%). Recrystallization from HOAc afforded a lustrous red crystalline powder, dec > 265 °C. IR: 1498 (m), 1447 (s), 1434 (s), 1430 (s), 1350 (s), 1273 (s), 1237 (s), 1171 (m), 1075 (w), 1027 (s), 990 (w), 874 (m), 838 (m), 793 (m), 759 (w), 735 (w), 707 (s), 655 (s), 638 (s), 583 (w), 573 (w), 534 (w), 516 (m) cm⁻¹. Anal. calcd for C₈H₅BrF₃N₃O₃S₃Se₂: C, 16.50; H, 0.87; N, 7.22. Found: C, 16.40; H, 1.0; N, 7.14.

Preparation of 8-Bromo-4-ethyl-4H-bis[1,2,3]diselenazolo[4,5-*b*:5',4'-*e*]pyridin-2-ium Triflate, [4b][OTf]. Finely ground selenium dioxide (0.700 g, 6.31 mmol) was added to a hot solution of [3b][OTf] (1.22 g, 2.10 mmol) in 220 mL HOAc, and the reaction mixture was heated at reflux for 2 h. The heat was removed and the brown solution was cooled slowly to room temperature. After 16 h the red solid of [4b][OTf] was filtered off and washed with 20 mL DCM, yield 0.902 g (1.33 mmol, 64%).

The product was recrystallized from HOAc and isolated as purple needles, dec > 258 °C. IR: 2251 (w, MeCN), 1483 (w), 1417 (s), 1353 (s), 1318 (w), 1280 (s), 1244 (s), 1221 (s), 1176 (w), 1152 (s), 1085 (w), 1058 (w), 1026 (s), 985 (w), 894 (w), 774 (w), 759 (w), 735 (m), 712 (m), 699 (s), 637 (s), 581 (s), 572 (m), 566 (m), 532 (m), 516 (m) cm⁻¹. Anal. calcd for C₈H₅BrF₃N₃O₃S₃Se₄: C, 14.21; H, 0.75; N, 6.22. Found: C, 14.10; H, 0.63; N, 6.21.

Preparation of 8-Bromo-4-ethyl-4H-bis[1,2,3]diselenazolo[4,5-*b*:5',4'-*e*]pyridin-3-yl, 4b. *Method 1.* The electrocrystallization experiments employed standard electrochemical H-cell techniques,⁴² with samples of [4b][OTf] (25 mg) dissolved under nitrogen in 20 mL MeCN containing 8.0 × 10⁻³ M [n-Bu₄N][PF₆] as supporting electrolyte. Currents ranged from 5 to 10 μA, with growth periods of 2–4 days.

Method 2. Degassed (4 freeze–pump–thaw cycles) solutions of TMEDA (0.069 g, 0.420 mmol) in 50 mL MeCN and [4b][OTf] (0.200 g, 0.296 mmol) in 200 mL MeCN were combined and after 30 min the gold-brown precipitate of **4b** was filtered off and washed with 4 × 20 mL MeCN, yield 0.143 g (0.271 mmol, 92%), dec > 120 °C. IR: 1448 (s), 1397 (m), 1366 (m), 1349 (w), 1315 (m), 1223 (s), 1167 (m), 1079 (w), 1053 (w), 988 (m), 875 (w), 811 (w), 703 (w), 687 (s), 563 (m), 517 (w), 422 (w) cm⁻¹. Anal. calcd for C₇H₅BrN₃Se₄: C, 15.96; H, 0.96; N, 7.98. Found: C, 16.12; H, 1.09; N, 8.07.

Single Crystal X-ray Measurements. A needle of **4b** was glued to a glass fiber with epoxy. X-ray data were collected using omega scans on a Bruker SMART APEX CCD-based diffractometer using Cu Kα ($\lambda = 1.54178 \text{ \AA}$) radiation. The data were scanned using Bruker's SMART program and integrated using Bruker's SAINT software.⁴³ The structure was solved by direct methods using SHELXS-90⁴⁴ and refined by least-squares methods on F² using SHELXL-97⁴⁵ incorporated in the SHELXTL⁴⁶ suite of programs.

High Pressure X-ray Measurements. High pressure X-ray diffraction experiments on **4a** and **4b** were performed at BL10XU, SPring-8, using synchrotron radiation ($\lambda = 0.51446 \text{ \AA}$ for **4a** and 0.61795 Å for **4b**) and powdered samples mounted in a diamond anvil cell, with helium as the pressure transmitting medium. The diffraction data were collected at room temperature and as a function of increasing pressure. A series of data sets (from 0 to 15 GPa) were indexed with XRDA⁴⁷ and DICVOL,⁴⁸ as provided in DASH 3.01.⁴⁹ It was evident that both compounds **4a** and **4b** at all pressures were isostructural with the ambient pressure structures, and the space group $P\bar{4}2_1m$ was selected. Starting with the molecular coordinates for **4a** taken from the 100 K, ambient pressure data set,^{20b} and those of **4b** taken from the ambient temperature and pressure data set described here, as the initial models, the structures were solved and refined using DASH. The powder solutions for $P < 10 \text{ GPa}$ were further refined by Rietveld⁵⁰ methods using the GSAS⁵¹ program package. Final Rietveld indices R_p and R_{wp} are listed in Table S1. Data from $2\theta = 3\text{--}20^\circ$ were refined with fixed atomic positions and isotropic thermal parameters with an assigned value of 0.025. Atomic positions were not further refined, and as a result, standard deviations for atomic coordinates are not available. Isotropic thermal parameters were only refined for the selenium atoms, where possible.

Ambient Pressure Transport Property Measurements. DC magnetic susceptibility measurements on **4b** were performed over the range 2–300 K on a Quantum Design MPMS SQUID magnetometer. AC susceptibility measurements were performed on an Oxford Instruments MagLab EXA. Four-probe temperature dependent conductivity measurements on **4b** were performed on pressed pellet samples (1 × 1 × 5 mm) using a Quantum Design PPMS instrument. Silver paint (Leitsilber 200) was used to apply the electrical contacts.

High Pressure Magnetic Measurements. Piston cylinder cell (PCC) AC magnetic susceptibility measurements on samples of **4a** and **4b** were performed over the pressure range 0–1.6 GPa in a SQUID magnetometer. The crystals were mixed with a pressure transmitting medium, Apiezon J oil, and held with a piece of lead as the manometer.

Pressure calibration was performed using the superconducting transition of lead. Diamond anvil cell (DAC) AC magnetic measurements were carried on both **4a** and **4b** using techniques and procedures described previously.⁵²

High Pressure Conductivity Measurements. The variation of the electrical resistance of **4a** and **4b** with pressure was investigated by the four-probe technique in a diamond anvil cell. Pressure was generated by a pair of diamonds with a 600 μm diameter culet. A sample hole of 300 μm diameter was drilled in the gasket after its thickness was reduced from 250 to 30 μm by preindentation. It was then covered with a thin layer of cubic boron nitride BN for electrical insulation between the gasket and the electrodes. Gold wire of 18 μm diameter was used as electrode leads. The pressure was determined by the ruby fluorescence method at room temperature before and after each cooling cycle. Raw resistance measurements were converted into conductivity values by calibration with the ambient pressure 4-probe conductivity data.

■ ASSOCIATED CONTENT

Supporting Information. Details of X-ray crystallographic data collection and structure refinement, tables of atomic coordinates, bond distances and angles, anisotropic thermal parameters, and hydrogen atom positions in CIF format. Observed and calculated powder diffraction patterns for **4a** and **4b** as a function of pressure. Plots of conductivity of **4b** as a function of temperature and pressure. This information is available free of charge via the Internet at <http://pubs.acs.org>.

■ AUTHOR INFORMATION

Corresponding Author
oakley@uwaterloo.ca

■ ACKNOWLEDGMENT

We thank the Natural Sciences and Engineering Research Council of Canada (NSERC), MEXT of Japan, and NSF and MOST of China for financial support. We also thank the Japan Synchrotron Radiation Research Institute (JASRI) for beam time, NSERC for a Vanier Scholarship to K.L. and Canada Graduate Scholarships to A.A.L., S.M.W., and L.E.D., and the Government of Canada for a Tier I Canada Research Chair to J.S.T.

■ REFERENCES

- (a) Rawson, J. M.; Alberola, A.; Whalley, A. *J. Mater. Chem.* **2006**, *16*, 2560. (b) Hicks, R. G. *Org. Biomol. Chem.* **2007**, *5*, 1321. (c) Awaga, K.; Tanaka, T.; Shirai, T.; Umezono, Y.; Fujita, W. *C.R. Chimie* **2007**, *10*, 52. (d) Awaga, K.; Tanaka, T.; Shirai, T.; Fujimori, M.; Suzuki, Y.; Yoshikawa, H.; Fujita, W. *Bull. Chem. Soc. Jpn.* **2006**, *79*, 25. (e) Hicks, R. G. *Stable Radicals: Fundamentals and Applied Aspects of Odd-Electron Compounds*; John Wiley & Sons: New York, 2010.
- (a) Mito, M.; Nakano, H.; Kawae, T.; Hitaka, M.; Takagi, S.; Deguchi, H.; Suzuki, K.; Mukai, K.; Takeda, K. *J. Phys. Soc. Jpn.* **1997**, *66*, 2147. (b) Banister, A. J.; Bricklebank, N.; Lavender, I.; Rawson, J. M.; Gregory, C. I.; Tanner, B. K.; Clegg, W.; Elsegood, M. R. J.; Palacio, F. *Angew. Chem., Int. Ed.* **1996**, *35*, 2533.
- (a) Kinoshita, M.; Turek, P.; Tamura, M.; Nozawa, K.; Shiomi, D.; Nakazawa, Y.; Ishikawa, M.; Takahashi, M.; Awaga, K.; Inabe, T.; Maruyama, Y. *Chem. Lett.* **1991**, 1225. (b) Tamura, M.; Nakazawa, Y.; Shiomi, D.; Nozawa, K.; Hosokoshi, Y.; Ishikawa, M.; Takahashi, M.; Kinoshita, M. *Chem. Phys. Lett.* **1991**, *186*, 401. (c) Chiarelli, R.; Novak, M. N.; Rassat, A.; Tholence, J. L. *Nature* **1993**, *363*, 147. (d) Alberola, A.; Less, R. J.; Pask, C. M.; Rawson, J. M.; Palacio, F.; Oliete, P.; Paulsen, C.; Yamaguchi, A.; Farley, R. D.; Murphy, D. M. *Angew. Chem., Int. Ed.* **2003**, *42*, 4782.
- (4) Day, P. *Nature* **1993**, *363*, 113.
- (5) (a) Fujita, W.; Awaga, K. *Chem. Phys. Lett.* **2002**, *357*, 385. (b) Fujita, W.; Awaga, K. *Chem. Phys. Lett.* **2004**, *388*, 186.
- (6) Allemand, P. M.; Khemani, K. C.; Koch, A.; Wudl, F.; Holczer, K.; Donovan, S.; Gruner, G.; Thompson, J. D. *Science* **1991**, *253*, 301.
- (7) (a) Haddon, R. C. *Nature* **1975**, *256*, 394. (b) Haddon, R. C. *Aust. J. Chem.* **1975**, *28*, 2333. (c) Haddon, R. C. *Aust. J. Chem.* **1975**, *28*, 2343.
- (8) Hubbard, J. *Proc. Roy. Soc. (London)* **1963**, *A276*, 238.
- (9) (a) Mott, N. F. *Proc. Phys. Soc. A* **1949**, *62*, 416. (b) Mott, N. F. *Metal-insulator Transitions*; Taylor and Francis: London, 1990.
- (10) In Hartree-Fock theory, this condition becomes $W > (\pi/4)U$. See Whangbo, M. H. *J. Chem. Phys.* **1979**, *70*, 4763.
- (11) (a) Tian, Y.-H.; Huang, J.; Kertesz, M. *Phys. Chem. Chem. Phys.* **2010**, *12*, 5084. (b) Huang, J.; Sumpter, B. G.; Meunier, V.; Tian, Y.-H.; Kertesz, M. *Chem. Mater.* **2011**, *23*, 874. (c) Miller, J. S.; Novoa, J. J. *Acc. Chem. Res.* **2007**, *40*, 189. (d) Oakley, R. T. *Prog. Inorg. Chem.* **1988**, *36*, 399.
- (12) Peierls, R. C. *Quantum Theory of Solids*; Oxford University Press: London, 1955; p 108.
- (13) (a) Chi, X.; Itkis, M. E.; Patrick, B. O.; Barclay, T. M.; Reed, R. W.; Oakley, R. T.; Cordes, A. W.; Haddon, R. C. *J. Am. Chem. Soc.* **1999**, *121*, 10395. (b) Pal, S. K.; Itkis, M. E.; Tham, F. S.; Reed, R. W.; Oakley, R. T.; Haddon, R. C. *Science* **2005**, *309*, 281. (c) Mandal, S. K.; Samanta, S.; Itkis, M. E.; Jensen, D. W.; Reed, R. W.; Oakley, R. T.; Tham, F. S.; Donnadieu, B.; Haddon, R. C. *J. Am. Chem. Soc.* **2006**, *128*, 1982. (d) Pal, S. K.; Itkis, M. E.; Tham, F. S.; Reed, R. W.; Oakley, R. T.; Haddon, R. C. *J. Am. Chem. Soc.* **2008**, *130*, 3942.
- (14) (a) Haddon, R. C.; Sarkar, A.; Pal, S. K.; Chi, X.; Itkis, M. E.; Tham, F. S. *J. Am. Chem. Soc.* **2008**, *130*, 13683. (b) Bag, P.; Itkis, M. E.; Pal, S. K.; Donnadieu, B.; Tham, F. S.; Park, H.; Schlueter, J. A.; Siegrist, T.; Haddon, R. C. *J. Am. Chem. Soc.* **2010**, *132*, 2684. (c) Huang, J.; Kertesz, M. *J. Am. Chem. Soc.* **2003**, *125*, 13334. (d) Huang, J.; Kertesz, M. *J. Am. Chem. Soc.* **2007**, *129*, 1634. (e) Bohlin, J.; Hansson, A.; Stafstrom, S. *Phys. Rev. B* **2006**, *74*, 155111.
- (15) (a) Cordes, A. W.; Haddon, R. C.; Oakley, R. T. In *The Chemistry of Inorganic Ring Systems*; Steudel, R., Ed.; Elsevier: Amsterdam, 1992; p 295. (b) Cordes, A. W.; Haddon, R. C.; Oakley, R. T. *Adv. Mater.* **1994**, *6*, 798. (c) Oakley, R. T. *Can. J. Chem.* **1993**, *71*, 1775.
- (16) ΔH_{disp} is the enthalpy change for the conversion of two gas phase radicals R into a cation/anion pair, that is, $2 \text{R} \rightleftharpoons \text{R}^+ + \text{R}^-$ and is equal to the difference between the ionization potential (IP) and electron affinity (EA). The cell potential $E_{\text{cell}} = E_{1/2}(\text{ox}) - E_{1/2}(\text{red})$ is the difference between the half-wave potentials for the oxidation and reduction processes.
- (17) (a) Cordes, A. W.; Haddon, R. C.; Oakley, R. T. *Phosph., Sulf., Silicon Relat. Elem.* **2004**, *179*, 673. (b) Beer, L.; Brusso, J. L.; Cordes, A. W.; Haddon, R. C.; Itkis, M. E.; Kirschbaum, K.; MacGregor, D. S.; Oakley, R. T.; Pinkerton, A. A.; Reed, R. W. *J. Am. Chem. Soc.* **2002**, *124*, 9498.
- (18) (a) Brusso, J. L.; Derakhshan, S.; Itkis, M. E.; Kleinke, H.; Haddon, R. C.; Oakley, R. T.; Reed, R. W.; Richardson, J. F.; Robertson, C. M.; Thompson, L. K. *Inorg. Chem.* **2006**, *45*, 10958. (b) Brusso, J. L.; Cvrlj, K.; Leitch, A. A.; Oakley, R. T.; Reed, R. W.; Robertson, C. M. *J. Am. Chem. Soc.* **2006**, *128*, 15080.
- (19) Leitch, A. A.; Brusso, J. L.; Cvrlj, K.; Reed, R. W.; Robertson, C. M.; Dube, P. A.; Oakley, R. T. *Chem. Commun.* **2007**, 3368.
- (20) (a) Robertson, C. M.; Myles, D. J. T.; Leitch, A. A.; Reed, R. W.; Dooley, D. M.; Frank, N. L.; Dube, P. A.; Thompson, L. K.; Oakley, R. T. *J. Am. Chem. Soc.* **2007**, *129*, 12688. (b) Robertson, C. M.; Leitch, A. A.; Cvrlj, K.; Reed, R. W.; Myles, D. J. T.; Dube, P. A.; Oakley, R. T. *J. Am. Chem. Soc.* **2008**, *130*, 8414.
- (21) (a) Žutić, I.; Fabian, J.; Das Sarma, S. *Rev. Mod. Phys.* **2004**, *76*, 323. (b) Vardenny, Z. V. *Organic Spintronics*; CRC Press: Boca Raton, 2010.
- (22) Leitch, A. A.; Yu, X.; Winter, S. M.; Secco, R. A.; Dube, P. A.; Oakley, R. T. *J. Am. Chem. Soc.* **2009**, *131*, 7112.

- (23) Robertson, C. M.; Leitch, A. A.; Cvrkalj, K.; Myles, D. J. T.; Reed, R. W.; Dube, P. A.; Oakley, R. T. *J. Am. Chem. Soc.* **2008**, *130*, 14791.
- (24) (a) Takeda, K.; Mito, M. In *Carbon-Based Magnetism*; Makarova, T., Palacio, F., Eds.; Elsevier: Amsterdam, 2005; pp 131–158. (b) Mito, M.; Kawae, T.; Hitaka, M.; Takeda, K.; Ishida, T.; Nogami, T. *Chem. Phys. Lett.* **2001**, *333*, 69.
- (25) Mito, M.; Komorida, Y.; Tsuruda, H.; Tse, J. S.; Desgreniers, S.; Ohishi, Y.; Leitch, A. A.; Cvrkalj, K.; Robertson, C. M.; Oakley, R. T. *J. Am. Chem. Soc.* **2009**, *131*, 16012.
- (26) (a) Bondi, A. *J. Phys. Chem.* **1964**, *68*, 441. (b) Dance, I. *New J. Chem.* **2003**, *27*, 22.
- (27) Carlin, R. L. *Magnetochemistry*; Springer-Verlag: New York, 1986.
- (28) The subsequent tail-off in χT on cooling below T_C is a result of magnetization saturation.
- (29) As a result of the contribution of spin–orbit effects from selenium to the g value of **4a** and **4b**, the observation of values of M_{sat} slightly greater than $1 \text{ N}\beta$, where $M_{\text{sat}} = gSN\beta$, is not unexpected.
- (30) (a) Mito, M.; Kawae, T.; Takumi, M.; Nagata, K.; Tamura, M.; Kinoshita, M.; Takeda, K. *Phys. Rev. B* **1997**, *56*, 14255. (b) Mito, M.; Deguchi, H.; Tanimoto, T.; Kawae, T.; Nakatsuji, S.; Morimoto, H.; Anzai, H.; Nakao, H.; Murakami, Y.; Takeda, K. *Phys. Rev. B* **2003**, *67*, 024427.
- (31) Imada, M.; Fujimori, A.; Tokura, Y. *Rev. Mod. Phys.* **1998**, *70*, 1039.
- (32) (a) Murata, K.; Kagoshima, S.; Yasuzuka, S.; Yoshino, H.; Kondo, R. *J. Phys. Soc. Jpn.* **2007**, *75*, 051015. (b) Saito, G.; Yoshida, Y. *Bull. Chem. Soc. Jpn.* **2007**, *80*, 1. (c) Limelette, P.; Wzietek, P.; Florens, S.; Georges, A.; Costi, T. A.; Pasquier, C.; Jérôme, D.; Mézière, C.; Batail, P. *Phys. Rev. Lett.* **2003**, *91*, 016401. (d) Yasuzuka, S.; Murata, K. *Technol. Adv. Mater.* **2009**, *10*, 024307.
- (33) (a) Kahn, O. *Molecular Magnetism*; VCH: New York, 1993. (b) Kahn, O.; Briat, B. *J. Chem. Soc., Faraday Trans.* **1976**, *2*, 268. (c) Kahn, O.; Galy, J.; Journaux, Y.; Jaud, J.; Morgenstern-Badarau, I. *J. Am. Chem. Soc.* **1982**, *104*, 2165.
- (34) For details of the theoretical procedure, see (a) Noddleman, L.; Norman, J. *G. J. Chem. Phys.* **1979**, *70*, 4903. (b) Noddleman, L. *J. Chem. Phys.* **1981**, *74*, 5737. (c) Takano, Y.; Taniguchi, T.; Isobe, H.; Kubo, T.; Morita, Y.; Yamamoto, K.; Nakasui, K.; Takui, T.; Yamaguchi, K. *Chem. Phys. Lett.* **2002**, *358*, 17. (d) Yamaguchi, K. In *Self-Consistent Field Theory and Applications*; Carbo, R., Klobukowski, M., Ed.; Elsevier: Amsterdam, 1990; p 727. (e) Deumal, M.; Robb, M. A.; Novoa, J. *J. Prog. Theor. Chem. Phys.* **2007**, *16*, 271.
- (35) Details of these calculations, which were performed at the UB3LYP/6-31G(d,p) level on a model radical **4** with $R_1 = R_2 = H$, may be found in refs 22 and 23.
- (36) Like **3a**, radical **3b** also orders as a spin-canted antiferromagnet, with T_N of 14 K. Leitch, A. A.; Oakley, R. T. unpublished results.
- (37) Mito, M.; Fujino, M.; Komorida, Y.; Deguchi, H.; Takagi, S.; Fujita, W.; Awaga, K. *J. Phys. Soc. Jpn.* **2008**, *77*, 124713.
- (38) The sign of $\Delta\varepsilon_k$ reflects the nature of the SOMO–SOMO overlap (bonding or antibonding) between neighboring radicals. Values of $\Delta\varepsilon_k$ were derived from tight-binding (EHT) calculations in which the intermolecular separation along the π -stack was set at $\delta = 3.5 \text{ \AA}$. With increasing compression, the value of δ decreases, as shown in Figure 5, and the SOMO–SOMO interaction increases.
- (39) Gurvitch, M. *Phys. Rev. B* **1981**, *24*, 7404.
- (40) Georges, A.; Kotliar, G.; Krauth, W.; Rozenberg, M. *J. Rev. Mod. Phys.* **1996**, *68*, 13.
- (41) Stewart, G. R. *Rev. Mod. Phys.* **1984**, *56*, 755.
- (42) (a) Ferraro, J. R.; Williams, J. M. *Introduction to Synthetic Electrical Conductors*; Academic: New York, 1987; p 25. (b) Stephens, D. A.; Rehan, A. E.; Compton, S. J.; Barkhau, R. A.; Williams, J. M. *Inorg. Synth.* **1986**, *24*, 135.
- (43) SAINT, version 6.22; Bruker Advanced X-ray Solutions, Inc.: Madison, WI, 2001.
- (44) Sheldrick, G. M. *Acta Crystallogr. A* **1990**, *46*, 467.
- (45) Sheldrick, G. M. *SHELXL-97, Program for the Refinement of Crystal Structures*; University of Gottingen: Gottingen, Germany, 1997.
- (46) *SHELXTL, Program Library for Structure Solution and Molecular Graphics*, version 6.12; Bruker Advanced X-ray Solutions, Inc.: Madison, WI, 2001.
- (47) Desgreniers, S.; Lagarec, K. *J. Appl. Crystallogr.* **1998**, *31*, 109.
- (48) Boultif, A.; Louer, D. *J. Appl. Crystallogr.* **2004**, *37*, 724.
- (49) David, W. I. F.; Shankland, K.; van de Streek, J.; Pidcock, E.; Motherwell, W. D. S.; Cole, J. C. *J. Appl. Crystallogr.* **2006**, *39*, 910.
- (50) Rietveld, H. M. *J. Appl. Crystallogr.* **1969**, *2*, 65.
- (51) Larson, A. C.; Von Dreele, R. B. *General Structure Analysis System (GSAS)*; Los Alamos National Laboratory Report LAUR 86–748; 2000.
- (52) Mito, M.; Hitaka, M.; Kawae, T.; Takeda, K.; Kitai, T.; Toyoshima, N. *Jpn. J. Appl. Phys.* **2001**, *40*, 6641.